 doi:10.20944/preprints202209.0149.v1

Article

Comparison of geogases in Cenozoic sedimentary environments

Gabriele M. Berberich[1*] and Martin B. Berberich[2]

[1] Wissenschaftlich-Technisches Redaktionsbüro Dr. Berberich, Am Plexer 7, D-50374 Erftstadt, Germany - 1; gb@berberichweb.com; Orcid: 0000-0003-2656-7622
[2] IT-Consulting Berberich, Am Plexer 7, D-50374 Erftstadt, Germany; mb@berberichweb.com; Orcid: 0000-0003-0499-1270
* Correspondence: gb@berberichweb.com;

Abstract: We investigated fault gases (helium, radon, CO_2) in two seismically active Cenozoic sedimentary environments: a) Meinweg (in 2015) at a tectonically quiet horst structure in the Lower Rhine Embayment and b) Bodanrück (in 2012; Lake of Constance) at the Molasse Basin and part of the Freiburg–Bonndorf–Bodensee Fault Zone (FBBFZ). Both study areas were selected because recent "GeoBio-Interactions" findings showed, that red wood ants (RWA) are biological indicators of otherwise undetected degassing systems. A total of 817 soil gas samples was analyzed. Currently, Meinweg can be considered "no ants land" due to the very low background-level geogas concentrations. Thus, anomalies (Rn-CO_2) weakly trending in NE-SW extension direction emerged. This could probably indicate the onset of (re)activation of the NE-SW trending (Variscan) structures or the development of new fractures as an aftershock process of the 1992 Roermond earthquake that occurred about 15 km to the west. Results at Bodanrück (3 RWA clusters and two RWA-free corridors) revealed degassing patterns in NW-SE and NNE-SSW directions in the clusters corresponding to re-activated and recent strike-slip fault systems. No gas anomalies were found in RWA-free corridors. The RWA nest distribution was shown to be a valuable tool for identifying areas of even actively degassing spotty anomalies caused by macro- and microscale brittle deformation masked by sediment cover.

Keywords: soil gas anomalies; Helium, Radon, CO_2; Lower Rhine Embayment (LRE); Meinweg; Roer Valley Rift System (RVRS); Molasse Basin; Bodanrück; Freiburg–Bonndorf–Bodensee Fault Zone (FBBFZ); GeoBio-Interactions

1. Introduction

Soil gas analyses can be used to semi-quantitatively detect subsurface fault structures and crustal deformations in seismically active areas. The most important gases are noble gases such as helium (He), radon (Rn), and carbon dioxide (CO_2) [1-3]. Helium is considered an ideal geochemical tracer for crustal fluid motion [4]. Radon can be used as an additional tracer providing a qualitative measure of gas migration [5,6]. CO_2 serves as a carrier gas for e.g., Rn, and is produced by deep processes such as mantle degassing or thermo-metamorphic reactions. CO_2 is an important fault indicator, especially in areas with extensional tectonics [7]. Through fault cuts and/or extensive macroscale and/or microscale fractures, these fluids can escape laterally and vertically to form linear fault-bound anomalies, irregularly-shaped diffuse or "halo" anomalies and irregularly-spaced plumes or "spot anomalies" [e.g., 8]. Therefore, gas-bearing properties of faults are not necessarily continuous along a tectonic structure [5,9]. However, in areas with several hundred meters of sediment cover, e.g., in the Lower Rhine Embayment (LRE) or the Alpine Molasse Basin, it is difficult to detect buried fault structures.

 doi:10.20944/preprints202209.0149.v1

A recent research approach, "GeoBio-Interactions", that examined a combination of geoscientific and biological factors, found that red wood ants (*F. rufa*-group; hereafter RWA) can be used as a tool and biological indicators for otherwise undetected degassing systems and faults [10,11]. RWA nests were eight times more likely to be found within 60 m of known tectonic faults [12]. The results also showed that geogenic gases [13], rock formations with elevated Rn concentrations [14], fault-related CH_4 emissions [15], volatile organo-halogens, alkanes and limonene [16] play key roles in the settlement of RWA nests. Physical phenomena such as tectonic stress variations in the subsurface, leading to highly mobile and oxidizing electronic charge carriers and formation of H_2O_2 that flow to the surface [17,18] may contribute to the survival of the colony. Ants selectively consume harmful reactive oxygen species, such as H_2O_2 upon exposure to a fungal pathogen [16,19]. Furthermore, the ability of RWA to detect CO_2-concentrations in the soil [20,21] may provide an evolutionary advantage in site selection and nest establishments, positively influence and support pupal respiration metabolism [22] and the discontinuous breathing [23,24]. This "GeoBio-Interactions" approach also provides a satisfactory explanation for closely adjacent hot spots of RWA nests numbers and RWA free areas ("no ants land") in otherwise uniform forests.

Soil gas analyses were conducted in two separate but geologically and seismically comparable Cenozoic sedimentary environments a) Meinweg (MW) in the Lower Rhine Embayment (LRE) and b) Bodanrück (BR) in the the Freiburg–Bonndorf–Bodensee Fault Zone (FBBFZ). Both study areas had hot spots of RWA nests numbers (BR) and areas with no RWA nests (BR, MW). We wanted to investigate whether a combination of soil gas anomalies, presence/absence patterns of RWA nests and statistically analyzed preferred alignments directions of RWA nests (prototype lines; [10,11]) could add to the knowledge of degassing processes and fault systems in the two study areas. There is limited outcrop in both areas due to land cover, vegetation (forest stands and/or agriculture), sediments, or construction. Thus, current knowledge of the tectonic regime is indeed limited and/or incomplete.

We therefore tested our hypothesis that even in sedimentary environments with deposits being hundreds of meters thick (1) RWA preferentially establish and maintain their nests only on sites with gas anomalies for the fault gases (helium, radon, CO_2), and that (2) areas with no RWA nests do not show any soil gas anomalies for helium, radon, CO_2.

2. Materials and Methods

2.1 Location and tectonic settings of study areas

We investigated fault gases (helium, radon, CO_2) in two Cenozoic sedimentary environments: a) the Meinweg study area in the LRE as part of the seismically active NW-SE trending Rhine Graben Rift System (RGRS) and b) the Bodanrück study area (Molasse Basin, Lake of Constance) as part of the seismically active NW-SE trending FBBFZ.

The Nature Park Meinweg (MW; 0.8 km^2; henceforth Meinweg; Fig. 1a) is located approx. 6 km northwest of Wegberg and 13 km east of Roermond (The Netherlands) on the southeastern edge of the Roer Valley Rift System (RVRS) as part of the LRE. The LRE consists of a cyclic, unconsolidated sequence of Neogene and Quaternary marine and fluviatile siliclastic sediments and lignite seams several hundred meters thick. The basin sediments are underlain by Devonian bedrock (e.g., [25,26]. Both, the RVRS and LRE are part of the large Cenozoic RGRS that crosses western and central Europe [27]. During the Cenozoic, complex tectonic processes set in that included subsidence (rates 0.08 – 2.0 mm a^{-1}), NE-SW-E horizontal extension (rates 0.4 – 2.0 mm a^{-1}), and uplift (rates 0.06 – 2.0 mm a^{-1}; e.g., [26,28-30]). The present NW-SE compressional stress direction (~133°; [30]) was established during the Middle and Late Miocene [31]. Numerous NW-SE trending syngenetic normal faults (Early Oligocene) with possible strike-slip component overprinted preexisting Paleozoic and Mesozoic structures and cut the LRE into several tectonic blocks, such as half-graben and horst structures [29, 32-34]. They also have a significant influence

 doi:10.20944/preprints202209.0149.v1

on regional groundwater flow [35] The LRE has been seismically active since the Oligocene, with historical events exceeding M_L>6.3 [36]. A recent intraplate earthquake (M_L = 5.9, depth 17 km, [37] with dip-slip mechanism occurred on April 13, 1992 near the Dutch town of Roermond and the Peel Boundary Fault (Fig. 1a). With more than 200 aftershocks, it was as one of the largest in central and NW Europe since historical times and was strongly felt in the border region of the Netherlands, Germany and Belgium [38]. This earthquake triggered seismic activity in the RGRS up to 40 km to the southeast and caused damage in several Dutch and German cities [39]. Meinweg, thus is located on the seismically inactive and stable tectonic horst of Brüggen and Erkelenz, which is bordered by normal faults, the Peelrand Boundary fault to the west and Tegelen fault to the east [31,36]. Meinweg is located approx. 15 km east of the site of the Roermond earthquake. Meinweg can be designated as "no ants land" for no RWA nest was mapped within the study area.

The Bodanrück (BR; 16 km²; Fig. 1b) is located in the northern Alpine foreland between the towns of Markelfingen (northwest) and Constance (southeast) in the FBFZ. The underlying Molasse Basin is filled by unconsolidated marine and fluviatile sediments (Upper and Lower Molasse deposits; down to about 1000 m depth). It was formed by the African-European convergence and subduction of the European Plate and a subsequent Late Cenozoic uplift of the Alps and their northern foreland [40]. Glacial cover and movements resulted in moraine deposits and numerous drumlins. The geologic profile of the Dingelsdorf petroleum drilling, approx. 2 km northeast of cluster 1, showed that the Molasse deposits are underlain by Jurassic (approx. 500 m thick), Triassic (800 m thick), Carboniferous (100 m thick) and Crystallin units. Quaternary gravels (Rinnenschotter) deposited in an approx. 1 km wide and NW-SW trending channel structure, that runs along the southern coast of the BR between Markelfingen and Constance form the main confined groundwater system [41].

Since the Paleozoic, the BR has been influenced by complex tectonic processes that continue into the Cenozoic, resulting in reactivated and rearranged pre-existing Palaeozoic crustal discontinuities (e.g., [41-43]). The recent compression-induced stress field in NNW-SSE direction (~170°) results in extensional faults (ENE-WSW to W-E direction) and NW-SE, NNE-SSW and N-S trending faults (e.g., [41,44-49]). The Mindelsee Fault (right lateral strike-slip; Fig. 1b) runs along the long axis of the BR in NW-SE direction. Uplift (up to 0.4 mm a^{-1}), subsidence (up to -0.8 mm a^{-1}), and horizontal movements (1.0-2.5 mm a^{-1}) were recorded [47,50,51]. Low to moderate seismicity (M_L<4.2) showed historical events exceeding M_L>5.0. Geochemical soil gas anomalies indicate crustal degassing along faults [13,16,45].

More than 2600 RWA nests, divided into three clusters of 1310 (cluster 1), 915 (cluster 2) and 400 nests (cluster 3), were inventoried. These clusters are separated by two approx. NNE-SSW trending RWA-free corridors with an average width of approx. 800 m The Mindelsee fault is limiting the three clusters to the NE [10].

Preprints (www.preprints.org) | NOT PEER-REVIEWED | Posted: 12 September 2022 doi:10.20944/preprints202209.0149.v1

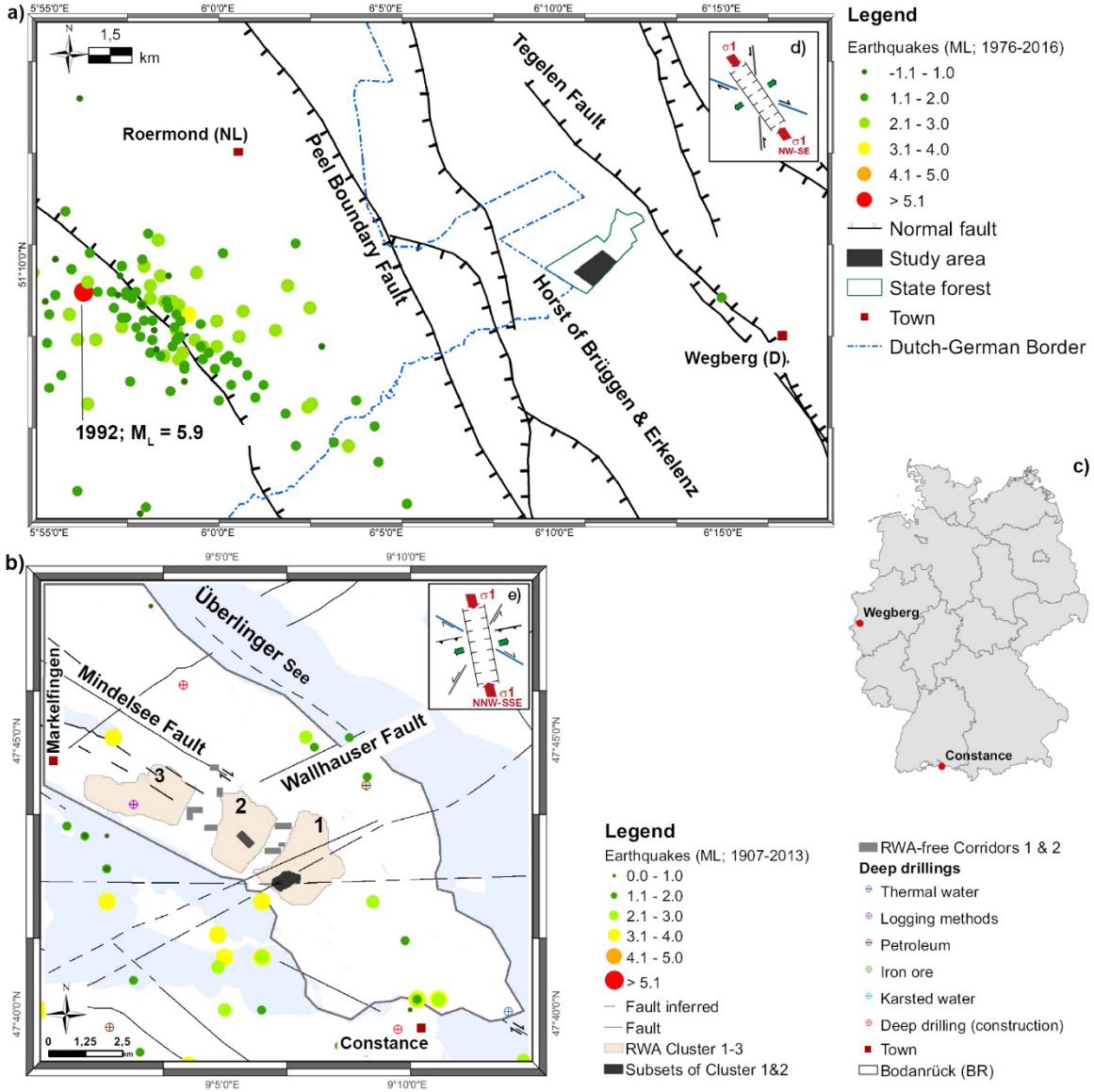

Figure 1. Location, tectonic structures (see list: compilation of tectonic structures) and earthquake events (see list of earthquake catalogues) of a) Meinweg and b) Bodanrück. Map (c) shows locations within Germany. Insets (d, e) show the tectonic standard models for both study areas [10].

2.2 Data collection

2.2.1 Soil gas sampling and geochemical analyses

In both study areas, a systematic sampling grid was placed depending on the area morphology and the number of RWA nests. A total of 817 soil gas samples was analyzed. In Meinweg a 75 m x 75 m sampling grid was used and a total of 222 samples were collected in spring 2015. At Bodanrück, a total of 427 soil gas samples (July 2011 and Mai 2012) were analyzed. The highest RWA nest numbers in cluster 1 & 2 determined the sample locations. A subset of cluster 1 (approx. 660 RWA nests on 40 ha; 337 gas samples) was sampled in a 60 m x 60 m sampling grid. Subset 2 in the center of cluster 2 (approx. 320 RWA nests on 15 ha; 90 gas samples) was sampled in slightly different sampling grid (50 m x 80 m; 90 gas samples) due to the presence of surface water (Fig. 1b; Table 1; [10]). Cluster 3 was only randomly sampled and is not part of this study. In addition, selected areas of the two RWA-free corridors were sampled (60 m x 60 m sampling grid; 168 gas samples, Table 1; [10]).

 doi:10.20944/preprints202209.0149.v1

Soil gas surveys were conducted during dry periods to avoid inference of meteorological factors [56]. The gases sampled were CO_2 and the two trace gases $helium_{tot}$ (hereafter He) and radon (Rn). Soil gas sampling followed the procedure described in [10] using a steel probe driven into the ground to a depth of 1 m. For He, a mobile, modified mass spectrometer (Alcatel ASM 142; adixen) was used on-site, which had been converted to a 20 ml sample volume for a single He-measurement. In parallel, standard air samples were analyzed to check the stability of the instrument. Since the samples may have been diluted by ambient atmospheric air during transfer from the syringe to the mass spectrometer, the measured residual He concentration was corrected accordingly. For Rn, 100 ml samples were transferred to evacuated, 100 ml capacity Lucas cells coated with ZnS(Ag) plates: they were analyzed after an interval of at least three hours using a Lucas detector (JP048; Radon Detector LUK4). To obtain a semi-quantitative measure of the gas leakage (CO_2) in the study area, a portable Dräger-meter equipped with a CO_2 sensor was successively operated for two minutes with soil gas samples (Dräger X-am ® 7000; DrägerSensor® Smart IR CO_2 HC, measuring range 0 – 100% by volume).

2.2.2 Collection of tectonic features

Information on tectonic features, such as published fault zones from geological maps (see list of geological maps this paper) of the study areas were transferred into a geographical information system.

2.3 Exploratory data analysis of soil gas

All collected information was entered into a database and processed. They were then analyzed geographically and statistically using R-Software (spatstat package [57] and ggplot2 version 1.11-7 [58] for R ([59]), Matlab 2015b (Surface fitting using gridfit function [60] and ArcGIS 10.3 software.

For the subsets 1 & 2 of both clusters, gas data were summarized for each gas studied to create a compact database for the analyses.

Exploratory data analysis (EDA) was performed in advance to statistically examine and evaluate the soil gas data using the procedure proposed by [61]. Tukey boxplots [62] were used to check for evidence of multiple populations (polymodality), and extreme or outlying values. Extremely high or low values that were separate from the main body of data were omitted, and a subset without these values was created. To test for normal distribution, the skewness of the data was estimated and Shapiro-Wilk [63] and t-test were calculated. Anomalous upper threshold values for the selected gases were calculated using the upper inner fence (UIF) of the boxplot [61,62] and the Median+2MAD [61] and compared to the mean ±2SD rule [64, 65]. The analysis of the sub-populations followed the procedure suggested by [66] but using the median+2MAD rule [61] because these estimators are robust to extreme values. To evaluate the strength of a linear relationship between paired data of possible gas associations, the data were lognormally transferred and the Pearson's correlation analysis [67] was performed with a level of significance of $p \leq 0.05$.

Gas data were then analyzed with respect to their spatial distribution, such as whether certain concentrations were clustered or randomly distributed. We used standard summary statistics, including, estimates of Ripley's K function [68], which estimate the expected number of random points within a distance r of a randomly chosen point in a plot, and the spatstat package for R to estimate K(r) for distances. Density plots were produced by using the background, threshold and maximum values and then compared to known structural features of known tectonic stress models.

3. Results

3.1 Gas composition

EDA of the soil gas survey for all studied areas (Table 1) showed a wide range of variations for some of the gas concentrations. This was particularly the case for Rn with

 doi:10.20944/preprints202209.0149.v1

concentrations ranging from 0 to 107 BqL^{-1} in the clusters and 1 to 87 BqL^{-1} in the corridors, but also for CO_2 in both clusters and corridors (0 – ~11 Vol. %).

 doi:10.20944/preprints202209.0149.v1

Table 1. Main statistical parameters of the soil gas surveys, definitions of an upper threshold via: Mean±2SD, upper inner fence (UIF) of a boxplot, and Median+2MAD and corresponding background values

Gas species	n	min	max	mean	median	SD	LQ	UQ	IQR	Skew-ness	Shapiro-Wilk test			*t* test (h)	Mean ±2SD	UIF	Median +2MAD	Back-ground values
											W	H	p					
a) Meinweg (n_{total}: 222)																		
He (ppm)	74	5.16	5.27	5.22	5.23	0.02	5.21	5.24	0.03	-0,40	0.96	1	0.01	1	5.27	5.29	5.27	5.22[a]
Rn (BqL^{-1})	74	0.00	17.00	5.00	4.00	4.00	3.00	7.00	4.00	1.04	0.91	1	<0.05	1	12.32	13.41	9.97	40[b]
CO_2 (Vol.%)	74	0.00	3.20	0.70	0.60	0.60	0.40	1.00	0.60	1.60	0.84	1	<0.05	1	1.91	1.90	1.49	<1.5[c]
a) Bodanrück																		
Subsets 1 & 2 of cluster 1 & 2 (n_{total}: 427)																		
He (ppm)	141	4.43	5.78	5.20	5.22	0.18	5.14	5.28	0.14	-0.36	0.91	1	<0.05	1	5.57	5.49	5.46	5.22[a]
Rn (BqL^{-1})	143	0.00	107.00	34.00	31.00	23.00	15.00	47.00	31.00	0.91	0.94	1	<0.05	1	80.16	93.58	66.62	23[d]
CO_2 (Vol.%)	143	0.00	10.80	2.00	1.60	1.60	1.00	2.60	1.60	2.40	0.79	1	<0.05	1	5.19	5.00	3.82	<1.5[c]
Corridors 1 & 2 (n_{total}: 168)																		
He (ppm)	56	2.34	5.37	5.13	5.17	0.38	5.14	5.21	0.07	-6.99	0.21	1	<0.05	1	5.89	5.31	5.39	5.22[a]
Rn (BqL^{-1})	56	1.00	87.00	34.00	25.00	25.00	13.00	55.00	42.00	0.49	0.92	1	<0.05	1	84.35	118.75	68.67	23[d]
CO_2 (Vol.%)	56	0.00	10.40	2.05	1.80	1.74	1.00	2.20	1.20	2.60	0.74	1	<0.05	1	5.52	4.00	3.91	<1.5[c]

[a][69]; [b][70]; [c][71] for non-volcanic areas; [d][72]

Preprints (www.preprints.org) | NOT PEER-REVIEWED | Posted: 12 September 2022 doi:10.20944/preprints202209.0149.v1

In all studied areas, the three gases (Rn, He, CO_2) were not normally distributed, which was confirmed statistically (*t* test h = 1; H = 1 Shapiro-Wilk test; $p \leq 0.05$). Geochemical data are generally right-skewed [61], and this was also true for the Rn and CO_2 data for all study areas. Very low values of negative skewness (-0.4) were found for He in Meinweg and both clusters. The high negative skewness (-6.99) for He in both corridors suggest that the non-normal distribution is strongly influenced by the large number of low concentrations (83%). The results (Table 1) illustrate that the mean±2SD [64,65] is generally not suitable for estimating the anomalous threshold [61], because these estimators are not robust to extreme values. This could be shown for the calculated anomalous He thresholds in both clusters. To capture outliers hidden in a lower population, the median+2MAD value suggested by [61] was considered more reliable and used for interpretation.

According to the Pearson correlation test (Table 2), the Rn-CO_2 couple for clusters 1 & 2 and for the subset within cluster 1 shows a strong relationship [73], whereas Meinweg and both BR corridors show only a weak to moderate relationship, respectively.

Table 2. Results of Pearson's correlation test (level of significance $p \leq 0.05$) for log-transformed soil gas data. Moderate to high positive relationships [73] are indicated in bold.

Gas	Meinweg			Bodanrück					
				Subsets of c luster 1 & 2			Corridors 1 & 2		
	He	**Rn**	**CO_2**	**He**	**Rn**	**CO_2**	**He**	**Rn**	**CO_2**
He	1			1			1		
Rn	-0.2	1		0.1	1		-0.0	1	
CO_2	-0.2	**0.5**	1	0.2	**0.7**	1	-0.0	0.4	1

3.1.1 Meinweg

No He anomalies were observed in Meinweg (Table 1), which was confirmed by statistical analyses. Although 51% of the He concentrations were above the atmospheric standard of 5.22 ppm [69], they all remained below the threshold of 5.27 ppm (Table 1; Fig. 2 and 3). Approximately 16% of the Rn concentrations were above the anomalous threshold of ~10 BqL^{-1}, and showed a tendency to cluster (Fig. 3). However, all observed Rn concentrations remained below the background concentrations of ~40 BqL^{-1} [70] for this study area. CO_2 concentrations were also very low, about 9.5 % of them exceeding the anomalous threshold (Fig. 2) of 1.5 Vol. %. A tendency towards clustering of Rn was observed only at distances greater than ~100 m.

3.1.2 Bodanrück

Q–Q plots for Bodanrück showed that most the gas species differ in shape, location and distribution (Fig. 2). The non-normal He distribution is strongly characterized by 47.5% of the data being below the constant atmospheric concentration (5,2204±0.0041 ppm; [69]). Two extreme He values in cluster 1 (~8.47 ppm) which could be clearly attributed to a mishandling in the analysis, were excluded from further investigations. He in clusters and Rn in corridors were bimodally distributed and represent sub-populations in both data sets. Analyses of the He sub-populations revealed five distinct anomaly classes: (1: concentrations above 5.61 ppm, 2: from 5.61 – 5.53 ppm, 3: 5.53 – 5.28 ppm, 4: 5.28 – 5.20 ppm, 5: concentrations below 5.20 ppm). The fifth class corresponds to the atmospheric standard of 5.22 ppm [69] and is considered as background levels for the entire population. Concentrations lower than background were considered to be undisturbed values [66]; all other anomaly classes indicated a tectonic influence. The analyses of the Rn sub-population also yielded anomaly classes (1: concentrations above 84 BqL^{-1}, 2: 84 – 76 BqL^{-1}, 3: 76 – 34 BqL^{-1}, 4: 34 – 28 BqL^{-1}). The anomalous threshold concentrations of categories 1-3 are up to 1.5 times higher than the estimated annual mean values for Germany (50 BqL^{-1}; [74]). Concentrations below 28 BqL^{-1} were addressed as background level and considered as undisturbed values [66]. This corresponds well to the value of 23 BqL^{-1}

Preprints (www.preprints.org) | NOT PEER-REVIEWED | Posted: 12 September 2022 doi:10.20944/preprints202209.0149.v1

published by [72]. The range of values between anomaly 1 and anomaly 4 indicates a tectonic influence and could reflect different lithological characteristics. The maximum Rn values (107 BqL^{-1}) were found at the northeast edge and center of the subset of cluster 1 and in the center of subset 2 of cluster 2. The CO_2 data had the highest values (11 and 9 Vol. % respectively) at the southwest edge of cluster 1 and in the center of cluster 2 (2,2 Vol. %). Approximately 8% of the CO_2 data were above the anomalous threshold of 4 Vol.% (cluster 1).

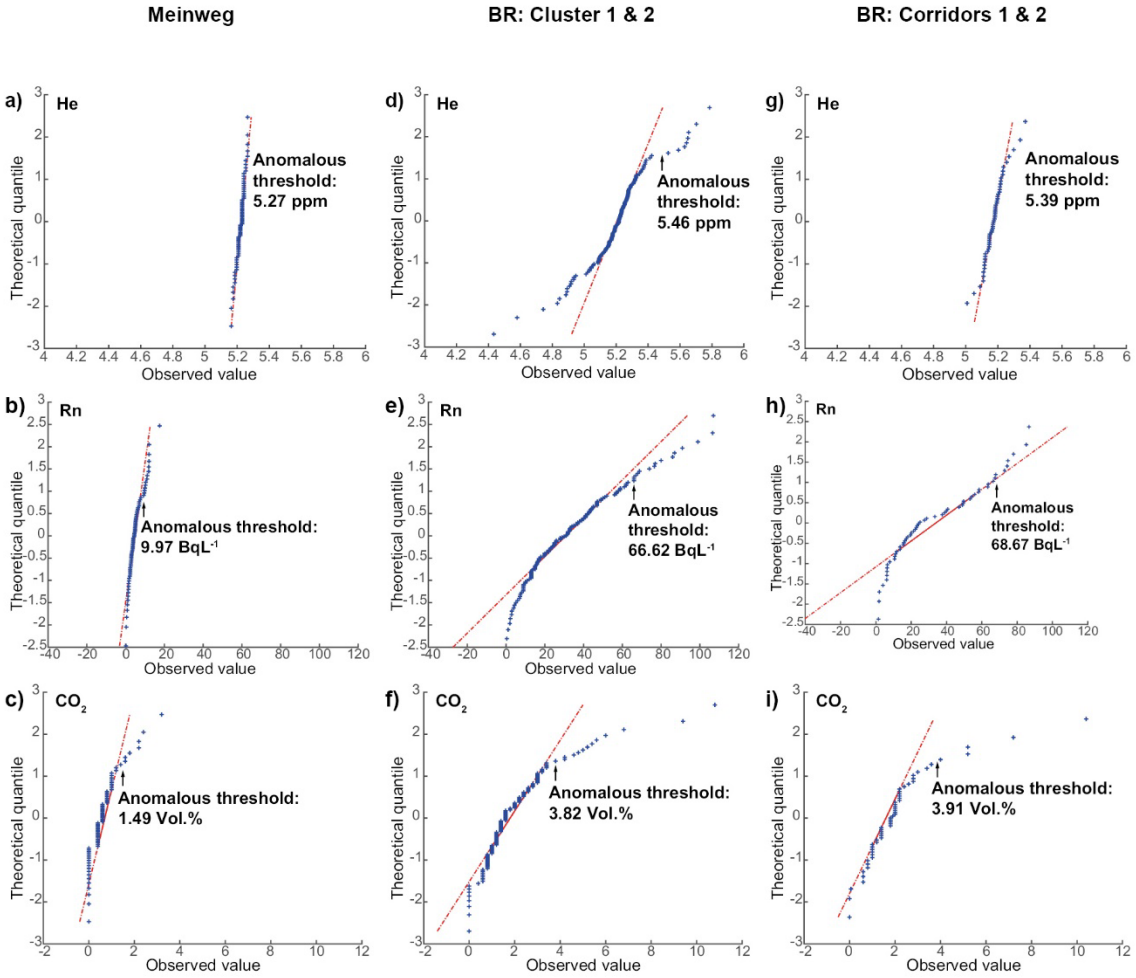

Figure 2. Quantile-quantile plots for He, Rn and CO_2, for Meinweg (a-c), BR clusters 1&2 (d-f) and BR corridors 1&2 (g-i) highlighting anomalous upper thresholds for the single gas species. The dashed red line is the theoretical cummultative distribution function.

To distinguish between random and cluster distributions, the observed gas concentrations were compared with 99 different random distributions with respect to the gas-specific anomalous thresholds (Fig .3). In the RWA-clusters, the observed values of all gases deviated significantly from a Poisson distribution, showing clustering at distances greater than ~60 m (above 5.20 ppm He and 28 BqL^{-1}) and greater than ~80 m for CO_2. In both corridors, only Rn a tendency to cluster at distances greater than ~120 m.

Preprints (www.preprints.org) | NOT PEER-REVIEWED | Posted: 12 September 2022 doi:10.20944/preprints202209.0149.v1

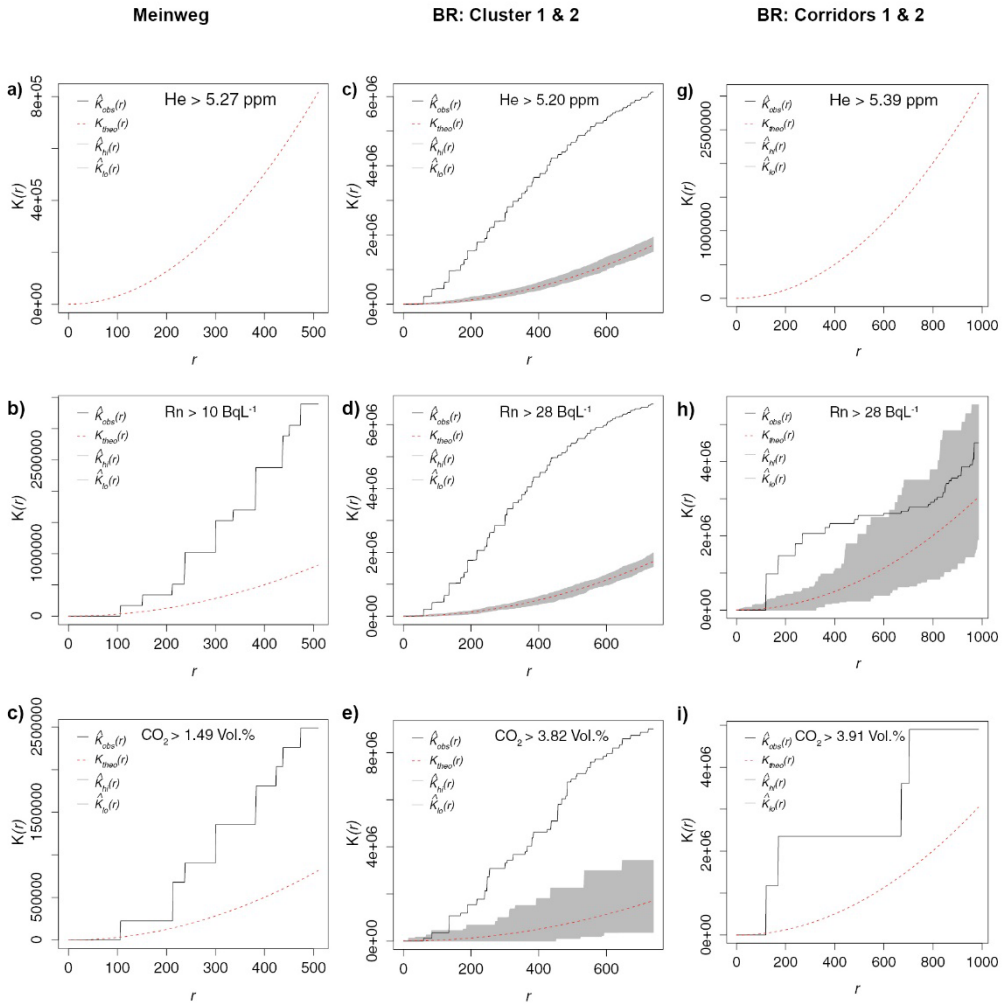

Figure 3. Estimated K-function curves for He, Rn and CO_2 for Meinweg (a-c), BR clusters 1&2 (d-f) and BR corridors 1&2 (g-i) compared to 99 different random distributions concerning the gas-specific anomalous thresholds. The behavior of the empirical means is indicated by solid black lines, the dashed red line is Ripley's K-function and grey areas are the confidence envelopes.

3.2 Spatial analyses

3.2.1 Meinweg

Surface plots of spatial degassing pattern in Meinweg revealed a weakly NE-SW trending direction for the Rn-CO_2 degassing couple (Fig. 4a,c).

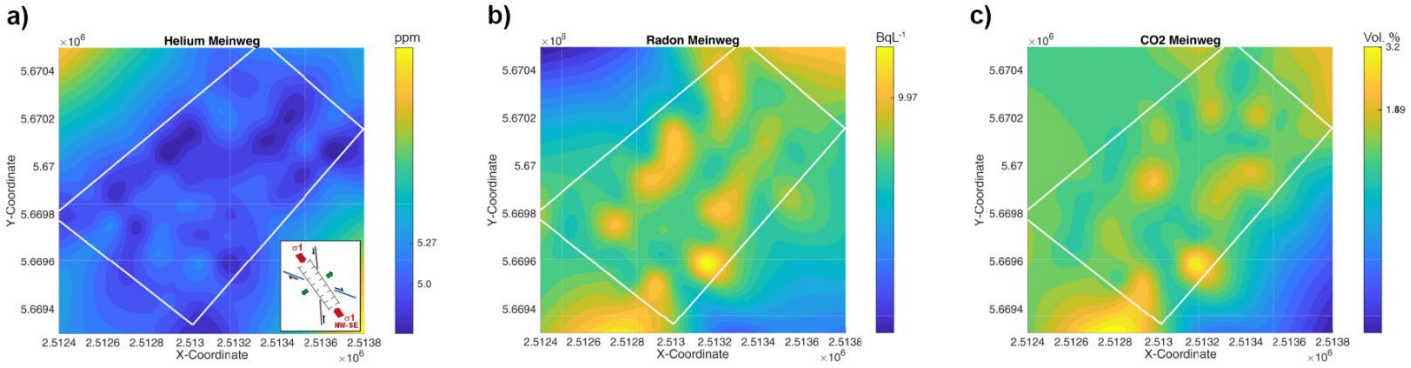

Preprints (www.preprints.org) | NOT PEER-REVIEWED | Posted: 12 September 2022 doi:10.20944/preprints202209.0149.v1

Figure 4. Surface maps of degassing patterns for RWA-free Meinweg area with respect to the background, anomalous threshold and maximum values for He (a), and anomalous threshold and maximum values for Rn (b) and CO_2 (c). Inlet shows the present-day stress field for the study area.

3.2.2 Bodanrück

Geostatistical analyses of spatial gas distribution for the two subsets at BR revealed spotty degassing patterns (Fig. 5a-f) that were not randomly distributed for all three gases. A NW-SE- and a NNE-SSW-trending degassing pattern was observed in the subset of cluster 1 and in the subset of cluster 2, respectively. Statistical analyses of RWA nest distribution pattern generated a set of RWA prototype lines, which are also trending in NNE-SSW directions. These lines are between approx. 25 m and 70 m away from the degassing spots. The spatial degassing directions in subset 2 of cluster 2 are less pronounced in NW-SE direction. RWA Prototypes trending in NW-SE directions are suggested to be the best. No degassing pattern was observed in either RWA-free corridor

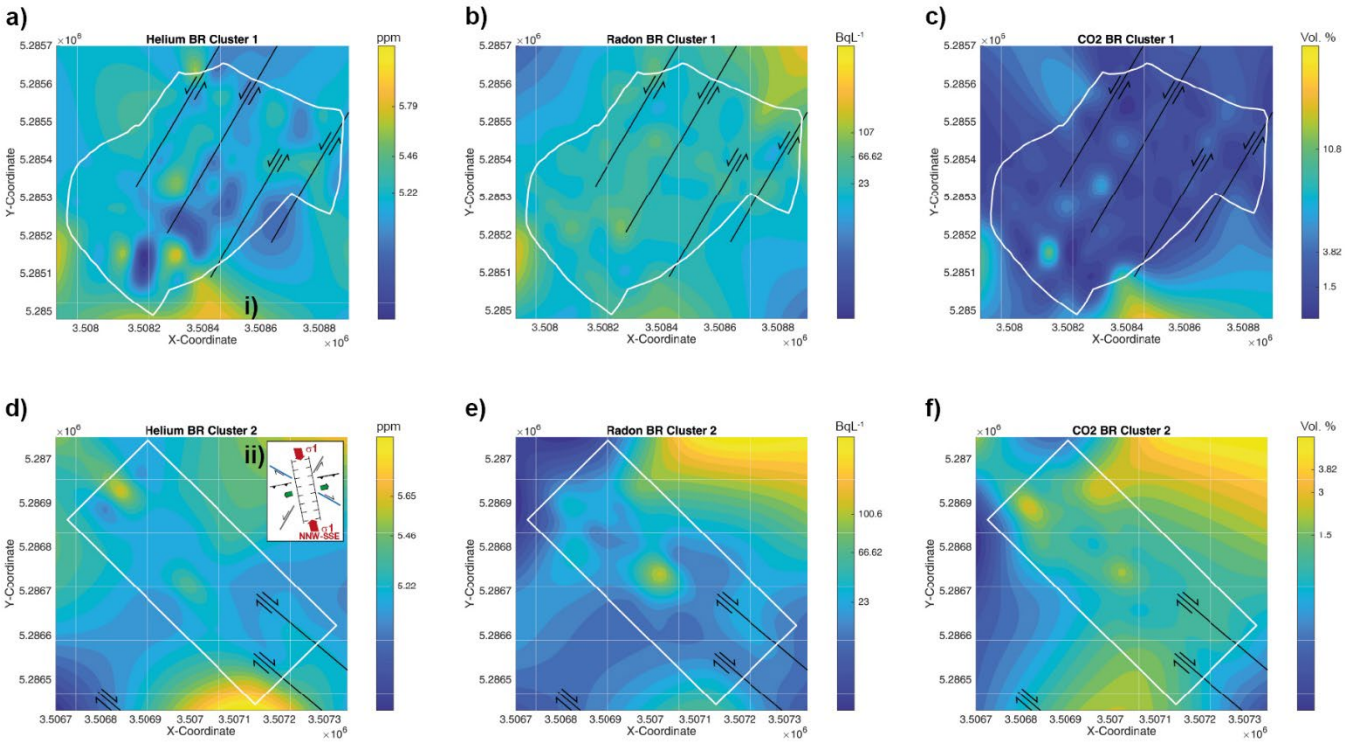

Figure 5. Surface maps of degassing patterns for subsets 1 (a-c) and subset 2 (d-f) of cluster 1 & 2 at Bodanrück with respect to the background, anomalous threshold and maximum values for He (a), Rn (b) and CO_2 (c) in comparison with interpretation of re-activated strike-slip fault zones (black lines with black arrows) analysed from RWA prototype lines [10]. Black arrows indicating left-lateral strike slip mode for subset 1 and right-lateral strike slip mode for subset 2 according to [10,42]. Inlets show i) the Swabian-Franconian fault system of the Eocene-Oligocene [42] and ii) the the tectonic standard model for the Bodanrück area [10].

4. Discussion

Geogenic gases such as He, Rn, CO_2, can be used to detect tectonic systems, e.g., shear zones, open fractures, and other zones of increased permeability that were previously unknown, and to semi-quantitatively track tectonic activity in seismically active zones [3,75]. Thermal, radiogenic, and geodynamic processes can influence degassing processes, as well as fault intersections and/or extensive macro- and/or micro-scale fractures at faults, resulting in a complex degassing pattern [8,75]). In addition to continuous degassing

 doi:10.20944/preprints202209.0149.v1

patterns along a tectonic structure, irregularly shaped diffuse or "halo" anomalies and irregularly distributed plumes or "spot anomalies" may develop [5,9]. Furthermore, highly complex multi-layered sedimentary sequences of marine and fluviatile origin can influence spatial degassing patterns [35].

The diffuse degassing patterns detected in both study areas are due to the heterogenic sedimentary environments. Changing geological environments in the surroundings of a fault system may trap geogenic gases (e.g., impermeable layers), resulting in residual migration and spotty degassing anomalies [78,79].

The Rn–CO_2 couple, confirmed by statistical analyses, is a typical carrier-trace gas association [80]. In diffusive systems, given by the large thickness of clastic sediments at Meinweg and BR, Rn has low mobility [74]. Combined with its short half-life, migration from the deeper source rock is limited in the absence of a carrier gas. Spatial concurrency of the Rn–CO_2 concentrations provided evidence of this transport mechanism in Meinweg (Fig. 4) and the two BR clusters (Fig. 5). The correlation factors (Table 2) showed a strong relationship for areas with RWA, with higher values in areas with RWA occurrence than in areas without RWA occurrence. Correlation factors found in RWA areas are ~55% higher as compared to gas analyses of active normal faults in the Western Corinth Gulf Rift [81] and in the Tolfa region [82], confirming active degassing in both subsets of the BR clusters. The moderate to weak correlation factors of the Rn–CO_2 gas couple in the BR corridors and in Meinweg are comparable to the findings of [82].

4.1 Meinweg

The Meinweg study area, located on the horst of Brüggen & Erkelenz, can be considered tectonically quiet due to the absence of almost all earthquakes (Fig. 1a). This could be confirmed by the absence of He concentrations above the anomalous thresholds (5.27 ppm; Table 1 and Fig. 4a). These He values are also confirmed by the fact that 90.5% of the CO_2 concentrations were below 1.5 Vol.%. This is typical for non-volcanic areas and is consistent with rift basin processes [31,83]. The remaining 9.5% of the CO_2 samples were only moderately higher and centered between 1.5 and <5Vol.%. The low CO_2 concentrations could also be due to biological processes, such as the microbial decomposition of organic matter or root respiration, which could have a strong influence on the soil gas composition [82,84].

In addition, there was a moderate relationship between the Rn-CO_2 degassing couple yet (Table 2), although the Rn concentrations were beyond the background value of ~40 BqL^{-1} [70]. The estimated K function curves for Rn and CO_2 indicate some clustering (Fig. 3b,c) which can be confirmed by the surface plots showing degassing spots approximately in NE-SW direction (Fig. 4a,c). This observation would also confirm findings by [7] that CO_2 is a main fault indicator especially in areas with extensional tectonics. This is also well related to the extension direction of the present-day stress field in NE-SW direction according to the rifting process [31]. When seismicity increases due to the rifting process, the opening of degassing fracture zones will be further triggered [29]. Thus, the first evidences for a possible new degassing system in NE-SW direction was observed during our investigations, probably indicating the onset of (re)activation of the NE-SW trending (Variscan) structures or the emergence of new fracture zones as aftershocks of the 1992 Roermond earthquake (M 5.9; [37]). This was one of the largest earthquakes recorded in the LRE may have been the trigger for the onset of soil degassing processes on the seismically quiet horst of Brüggen & Erkelenz. In addition, overstepping faults in the deeper subsurface may have been triggered by this earthquake and may have led to a local reduction of the sealing effect of faults [25]. Meinweg is also located approx. 20 km northwest to the open-pit mine Garzweiler (lignite), where large-scale water withdrawals are occurring. This large-scale abstraction and associated lowering of the groundwater table have significant impacts on the regional aquifer system. Because the stratified aquifer system is intersected by numerous NW-SE striking faults that can act as both barriers and preferential flow paths for groundwater [35], these changing water tables could also

 doi:10.20944/preprints202209.0149.v1

contribute to the degassing process and explain the weak expression of the observed degassing pattern.

Currently, Meinweg can be considered "no ants land" as no RWA nests have been observed so far. One reason could be that the concentrations of the soil gas anomalies were too low, for RWA especially prefer substrates with higher Rn concentrations [14] as observed at Meinweg. If the rifting process, the (re-)activation of faults and a higher concentrated degassing continue, RWA nests could be observed in this area in the future. Such processes should be monitored regularly to detect the development of RWA nest foundations and thus new hot spots of degassing systems. The combination with regular gas monitoring should provide information on whether the assumed (re-)activation process of faults continues.

4.2.Bodanrück

Seismically active zones, such as the FBBFZ, are usually wide and can be intersected by other structures. Such zones with high He fluxes act as preferential conduits for trapped gases near the intersection of the fractures with the surface [5,76]. On the other hand, He can, accumulate strongly over time in suitable traps [77], e.g., basin fillings with high porosities.

At Bodanrück, the spotty degassing structures (Fig. 5) were not randomly distributed for all three gases. Marine or freshwater sediment fillings may trap the gas in the micropores by water films, which may act as a barrier to the He-migration, resulting in only spotty degassing [77]. The maximum (5.78 ppm) and minimum (4.43 ppm) concentrations of He in the RWA-clusters are both higher than in the tectonically active Tolfa mine district [82]. Both clusters are located in a geothermal area, that may be sources for He release in juvenile or circulating meteoric water [77]. Thermal water drillings in the adjacent towns Constance and Kreuzlingen showed similar water temperatures (29°C), that were 2°C to 3°C higher than the normal geothermal gradient for this depth [85]. The anomalous thresholds of Rn, which were similar for both clusters and corridors, suggest a common degassing input linked to local tectonics. Spotty anomalies of Rn and CO_2 in both clusters revealed the presence of degassing structures beneath the sediment cover at previously unknown depths. The high Rn concentrations suggest advective migration processes that preferentially pass through zones of brittle deformation [86], as suggested by the relatively high rate of migration required to obtain anomalies of short-lived Rn in the soil pores [82]. Peak Rn concentrations were twice the estimated annual mean for Germany (50 BqL^{-1}; [74] and four times the background concentration [72]. CO_2 is not only an important fault detector, but is also important for seismic and volcanic monitoring [87]. According to the CO_2 concentration exposure categories for diffuse degassing hazard maps [71], 47% (clusters) and 41% (corridors) of the CO_2 data show a signature of non-volcanic areas (<1.5 Vol.%), whereas 6% (clusters) and 7% (corridors) are above the threshold of 5 Vol.%, i.e., with lethal concentrations affecting the ecosystem [71,88]. Furthermore, the unusually high CO_2 anomaly peaks (10.8 Vol.% RWA-clusters, 10.4 Vol.% corridors) were comparable to values from the sediment-covered and hydrothermally influenced Tolfa mine district [82]. The higher CO_2 concentrations at could also be associated with the adjacent Hegau volcanic field (Late Neogene), located at the northwest boundary of BR as part of the seismically active FBBFZ ([47,89]. Other sources of CO_2 include metamorphism of carbonate-bearing rocks or minerals, biological activity or hydrocarbon degradation ([1,76,90]. Isotopic analysis of CO_2 could provide information on the origin of this gas.

In the subset of cluster 1, the gas anomalies for all three gases in the NNE-SSW direction were well related to the results of statistical analyses of the spatial distributions of RWA nests (prototype lines). Latter revealed the preferential nests alignment in NNE-SSW direction, which can be addressed as re-activated left lateral-strike-slip fault systems (Eocene-Oligocene) of the Swabian-Franconian fault system (main stress direction σ1: 170°; [10,42]; Fig. 5a-c,i). This direction resembles the present-day stress-system with a

 doi:10.20944/preprints202209.0149.v1

left-lateral-strike-slip fault system as a conjugate shear system. The degassing pattern also followed this conjugate shear system. The supposed fault lines in NE-SW and W-E directions and at different, flatter angles [45] could not be confirmed by our "GeoBio-Interaction" approach.

The spatial degassing directions in subset 2 of cluster 2 are less pronounced in NW-SE direction (Fig. 5d-e). The NW-SE trending anomalies also agreed well with the trend of published structural features, and are consistent with the general NW-SE fault orientation (maxima at 135°–145°) in this area. This is also in good agreement with the NW-SE right-lateral strike-slip system of the large-scale Mindelsee fault zone (conjugated shear system to the present-day main stress direction; [41] that had been identified on parts of the BR, and with an assumed right-lateral strike-slip fault along the length of the Lake Constance (Fig, 1b; [48,49]. Therefore, the NW-SE direction of the analyzed prototype lines from RWA nests can be interpreted as right-lateral strike-slip fault systems (conjugated shear system) to the present-day main stress direction (Miocene/Pliocene-recent: σ1: 135°; Fig. 5d-e; [10,42]. At BR, the findings by [7] could not be confirmed, because the degassing patterns of CO_2 as main fault indicator were not observed in the extension direction.

Both RWA-free corridors can be addressed as "no ants land". Here, there is no tectonically influenced signature by the fault zone tracer He, as the observed He values do not exceeded the anomalous threshold (5.39 ppm). The highest CO_2 value (10.4 Vol. %) was found in corridor 2. About 7% of these CO_2 values exceeded the anomalous threshold of 4 Vol.%. The most common geological scenario for the occurrence of high CO_2 concentrations are deep faults near to gas traps, reservoirs close to hot bedrock and carbonates associated with post-trap igneous activity [91]. In addition, it is suggested that previously unknown tectonic fault structures, trending NNE-SSW to NE-SW (e.g., Wallhauser fault; Fig. 1b), may act as barriers and separate the degassing pattern in both clusters, consistent with a conduit-barrier model in unconsolidated sedimentary deposits as proposed by [35] for the LRE.

From our study, we conclude that the patterns of presence/absence of RWA nests and underlying geochemical anomalies are statistically significant even in sedimentary environments with deposits being hundreds of meters thick. This is especially valuable in areas where actively degassing tectonic systems are masked by heterogeneous sedimentary environments so far. Soil gas anomalies in areas with RWA nests confirmed that the spatial distribution patterns of RWA nests reflect a) the main tectonic fault directions of the present-day stress field with its accompanying conjugated shear systems but also b) previously unknown re-activated shear systems from earlier geological epochs [10]. In contrast, RWA were not present in areas without any soil gas anomalies.

5. Conclusion

Systematic sampling grids across both study areas showed a relation between gas anomalies and the spatial distribution of RWA nests. This trend-free procedure and our statistical analyses support our hypothesis: RWA addicted to geogenic soil gases. Areas without soil gas anomalies are "no ants land", regions where RWA nests are scarce. The relation between the spotty anomalies caused by macro- and micro-scale brittle deformation [86], and the RWA-prototype lines [10] confirmed RWA nests are a useful tool and are bioindicators to detect areas of even actively degassing spotty anomalies caused by macro- and microscale brittle deformation masked by sediment cover. The presence and composition of soil gas is one factor of the underlying mechanisms driving the alignment patterns of RWA nests. In addition, our results confirmed previous findings by [12], that RWA nests were eight times more likely to be found within 60 m of tectonic faults. This is especially valuable for areas with several hundred meters of sediment cover.

Author Contributions: GMB and MBB conducted fieldwork, performed statistical analyses and wrote the manuscript.

Funding: This research received no external funding.

Data Availability Statement: Data will be provided on demand.

Acknowledgements: The field work and analyses were conducted during the time, the first and corresponding author (Gabriele M. Berberich) was research associate of the University of Duisburg-Essen. Gas analyses were run on equipment from the department of Geology at University of Duisburg-Essen. The authors want to thank Mark Schumann, Thomas Ewert, Felix Dacheneder, Tamara Blocks, Stefan Hüssler and Martin Wankum for performing soil gas sampling and analyses (all University of Duisburg-Essen at that time).

Conflicts of Interest: The authors declare no conflict of interest.

References

1. Wilkinson, M.; Haszeldine, R. S.; Fallick, A.E.; Odling, N.; Stoker, S. J.; Gatliff, R.W. **2009**. CO_2–mineral reaction in a natural analogue for CO_2 storage—implications for modeling. J. Sed. Res., 79: 486–494. doi:10.2110/jsr.2009.052.
2. Gilfillan, S.M.V.; Wilkinson, M.; Haszeldine, R. S.; Shipton, Z.K.; Nelson, S.T.; Poreda, R.J. **2011**. He and Ne as tracers of natural CO_2 migration up a fault from a deep reservoir. Intern. J. Greenhouse Gas Control., 5: 1507-1516. doi:10.1016/j.ijggc.2011.08.008.
3. Martinelli, G.; Tamburello, G. **2020**. Geological and Geophysical Factors Constraining the Occurrence of Earthquake Precursors in Geofluids: A Review and Reinterpretation. Front. Earth Sci., 8:596050. doi:10.3389/feart.2020.596050.
4. Ciotoli, G.; Lombardi, S.; Morandi, S.; Zarlenga, F. **2004**. A multidisciplinary statistical approach to study the relationships between helium leakage and neo-tectonic activity in a gas province: The Vasto Basin, Abruzzo-Molise (Central Italy). Am. Assoc. Petrol. Geol., 88: 355-372. Doi:10.1306/10210303001.
5. Voltattorni N.; Sciarra A.; Quattrocchi, F. **2010**. The Application of Soil-Gas Technique to Geothermal Exploration: Study of Hidden Potential Geothermal Systems. In: Proceedings of the „World Geothermal Congress". Bali (Indonesia), 25-29 April 2010, 1-7.
6. Ma, Y.; Bringemeier, D.; Scheuermann, A.; Molebatsi, T.; Li, L. **2012**. Fault and fracture zone detection based on soil gas mapping and gamma ray survey at the extension site of an open pit coal mine, 12th Coal Operators' Conference, University of Wollongong & The Australasian Institute of Mining and Metallurgy, 378-386.
7. Tamburello, G.; Pondrelli, S.; Chiodini, G.; Rouwet, D. **2018**. Global-scale control of extensional tectonics on CO_2 earth degassing. Nat. Commun. 9, 4608. doi:10.1038/s41467-018-07087-z.
8. Ciotoli, G.; Lombardi, S.; Zarlenga, F. **2006**. Natural leakage of helium from Italian sedimentary basins of the Adriatic structural margin. Perspectives for geological sequestration of carbon dioxide. In: Advances in the Geological Storage of Carbon Dioxide, S. Lombardi et al., Eds.; Springer, The Netherlands,pp.191–202.
9. Ciotoli, G.; Lombardi, S.; Annunziatellis, A. **2007**. Geostatistical analysis of soil gas data in a high seismic intermontane basin: Fucino Plain, central Italy, J. Geophys. Res., 112: B05407. doi:10.1029/2005JB004044.
10. Berberich, G. M.; Grumpe, A.; Berberich, M.B.; Klimetzek, D.; Wöhler, C. **2016**. Are red wood ants (Formica rufa-group) tectonic indicators? A statistical approach. Ecol. Ind. 61: 968-979. doi:10.1016/j.ecolind.2015.10.055
11. Berberich, G. M.; Klimetzek, D.; Paraschiv, M.; Stancioiu, P.T.; Grumpe, A. **2019**. Biogeostatistics confirm: Even a low total number of red wood ant nests provide new information on tectonics in the East Carpathian Orogen (Romania). Ecological Indicators 101 (2019) 486–500. doi: 10.1016/j.ecolind.2019.01.005.
12. Del Toro, I.; Berberich, G. M.; Ribbons, R.R.; Berberich, M.B.; Sanders, N.J., Ellison, A.M. **2017.** Nests of red wood ants (Formica rufa-group) are positively associated with tectonic faults: a double-blind test. PeerJ 5:e3903. doi:10.7717/peerj.3903.
13. Berberich, G. M.; Berberich, M.B.; Ellison, A.M.; Wöhler, C. **2018**. Degassing Rhythms and Fluctuations of Geogenic Gases in A Red Wood-Ant Nest and in Soil in The Neuwied Basin (East Eifel Volcanic Field, Germany). Insects 2018, 9, 135. doi:10.3390/insects9040135.
14. Berberich, G. M.; Berberich, M.B.; Gibhardt, M. **2022**. Red wood Ants (Formica rufa-group) prefer mature pine forests in Variscan granite environments (Hymenoptera: Formicidae). Fragm. Entom., 54 (1): 1–18. doi:10.13133/2284-4880/474.
15. Berberich, G. M.; Ellison, A.M.; Berberich, M.B.; Grumpe, A.; Becker, A.; Wöhler, C. **2018**. Can a Red Wood-Ant Nest Be Associated with Fault-Related CH_4 Micro-Seepage? A Case Study from Continuous Short-Term In-Situ Sampling. Animals 2018, 8, 46; doi:10.3390/ani8040046.
16. Berberich, G. M.; Sattler, T.; Klimetzek, D.; Benk, S.A.; Berberich, M.B.; Polag, D.; Schöler, H.F.; Atlas, E. **2016**. Halogenation processes linked to red wood ant nests (Formica spp.) and tectonics. J Atmos Chem. doi:10.1007/s10874-016-9358-0.
17. Freund, F. **2011**. Pre-earthquake signals: underlying physical processes. J. Asian Earth Sci. 41: 383–400. doi:10.1016/j.jseaes.2010.03.009.
18. Freund, F.; Stolc, V., **2013**. Nature of pre-earthquake phenomena and their effects on living organisms. Animals 3: 513–531. doi:10.3390/ani3020513.
19. Bos, N.; Sundström, L.; Fuchs, S.; Freitak, D. **2015**. Ants medicate to fight disease. Evolution. doi:10.1111/evo.12752.
20. Kirchner, W. **2007**. Die Ameisen - Biologie und Verhalten. Verlag C.H. Beck, 125 Seiten.

21. Hölldobler, B.; Wilson, E.O. **2010**. Der Superorganismus – Der Erfolg von Ameisen, Bienen, Wespen und Termiten. Springer, Berlin, Germany. 604 p.
22. Schmidt, G. **1968**. Einfluss von Temperatur und Luftfeuchtigkeit auf die Energiebilanz während der Metamorphose verschiedener Kasten von *Formica polyctena* Foerst. (Hym.). Z. angew. Entom. 61: 61-109.
23. Lighton, J.R.B. **1988**. Discontinuous CO_2 Emission in a small insect. The Formicine Ant *Campoxotus vicixus*. J. Exp. Bio. 134: 363-376. Corpus ID: 87966359.
24. Hetz S.K.; Bradley, T.J. **2005**. Insects breathe discontinuously to avoid oxygen toxicity. Nature 433: 516-519. doi: 10.1038/nature03106.
25. Bense, V.F.; Van Balen, R.T.; De Vries, J.J. **2003**, The impact of faults on the hydrogeological conditions in the Roer Valley Rift System: an overview. Netherlands J. Geosc./Geol. en Mijnbouw 82 (1): 41-54. doi:10.1017/S0016774600022782.
26. Schäfer, A.; Utescher, T. **2014**. Origin, sediment fill, and sequence stratigraphy of the Cenozoic Lower Rhine Basin (Germany) interpreted from well logs. Z. Dt. Ges. Geowiss. (German J. Geosci.). 165: 287-314.
27. Ziegler, P.A. **1994**. Cenozoic rift system of western and central Europe: an overview. Netherlands J. Geosc./Geol. en Mijnbouw 73: 99-127. doi: 10.1016/0040-1951(92)90338-7.
28. Campbell, J.; Kümpel, H.-J.; Fabian, M.; Fischer, D.; Görres, B.; Keysers, Ch.J.; Lehmann, K. **2002**. Recent movement pattern of the Lower Rhine Embayment from tilt, gravity and GPS data. Netherlands J. Geosc./Geol. en Mijnbouw 81: 223-230. doi:10.1017/S0016774600022472.
29. Schäfer, A.; Siehl, A. **2002**. Preface: Rift tectonics and syngenetic sedimentation – the Cenozoic Lower Rhine Basin and related structures. Netherlands J. Geosc./Geol. en Mijnbouw. 81: 145-147. doi:10.1017/S001677460002237X.
30. Trautwein-Bruns, U.; Hilgers, C.; Becker, S.; Urai, J.L.; Kukla, P.A. **2011**. Fracture and fault systems characterising the intersection between the Lower Rhine Embayment and the Ardennes-Rhenish Massif results from the RWTH-1 well, Aachen, Germany. [Bruch- und Störungssysteme in der Übergangszone zwischen der Niederrheinischen Bucht und dem Rheinischen Schiefergebirge im belgisch-deutschen Grenzbereich Ergebnisse der Bohrung RWTH-1, Aachen, Deutschland]. Z. dt. Ges. Geowiss., 162: 251−276.
31. van Balen, R.T.; Houtgast, R.F.; Cloetingh, S.A.P.L. **2005**. Neotectonics of the Netherlands: a review. Quat. Sci. Reviews 24: 439–454. doi:10.1016/J.QUASCIREV.2004.01.011.
32. Hinzen, K.G. **2003**. Stress field in the Northern Rhine area, Central Europe, from earthquake fault plane solutions. Tectonophysics. 377: 325–356. doi:10.1016/j.tecto.2003.10.004.
33. Reamer, S.K.; Hinzen, K.G. **2004**. An earthquake catalogue for the northern Rhine Area, Central Europe (1975-2002). Seismol. Research Lett., 74: 575−582. doi: 10.1785/GSSRL.75.6.713.
34. Camelbeeck, T.; Vanneste, K.; Alexandre, P.; Verbeeck, K.; Petermans, K.; Petermans, T.; Rosset, P.; Everaerts, M.; Warnant, R.; Van Camp, M. **2007**. Relevance of active faulting and seismicity studies to assessments of long-term earthquake activity and maximum magnitude in intraplate northwest Europe, between the Lower Rhine Embayment and the North Sea. In: Continental intraplate earthquakes: science, hazard, and policy issues; Stein, S. & Mazzotti, S. Eds.; Geol. Soc. America, Spec. Pap., 425: 193−224.
35. Gumm, L.P.; Bense, V.F.; Dennis, P.F.; Hiscock, K.M.; Cremer, N.; Simon, S. **2015**. Dissolved noble gases and stable isotopes as tracers of preferential fluid flow along faults in the Lower Rhine Embayment, Germany. Hydrogeol J. doi:10.1007/s10040-015-1321-7.
36. Lehmann, K.; Klostermann, J.; Pelzing, R. **2001**. Paleoseismological Investigations at the Rurrand Fault, Lower Rhine Embayment. Netherlands J. Geosc./Geol. en Mijnbouw. 80: 139-154. doi:10.1017/S0016774600023805.
37. Van Eck, T.; Ahorner, L.; Paulssen, H. **1993**. The earthquake of the century in Northwestern Europe: the Roermond, the Netherlands, earthquake of April 13,1992. Earthquakes and Volcanoes (USGS) 24(1):15-26. doi:10.1016/0148-9062(95)94498-2.
38. Camelbeeck, T.; van Eck, T.; Pelzing, R.; Ahorner, L.; Loohuis, J.; Haak, H.W.; Hoang-Trong, P.; Hollnack, D. **1994**. The 1992 Roermond earthquake, the Netherlands, and its aftershocks. Netherlands J. Geosc./Geol. en Mijnbouw 73: 181-197, 1994.
39. Camelbeeck, T.; van Eck, T. **1994**. The Roer Valley Graben earthquake of 13 April 1992 and its seismotectonic setting. Terra Nova. doi:10.1111/j.1365-3121.1994.tb00499.x.
40. Andeweg, B.; Cloetingh, S.; **1998**. Flexure and 'unflexure' of the North Alpine German-Austrian Molasse Basin: constraints from forward tectonic modelling. In: Mascle, A., Puigdefabregas, C., Luterbacher, H.P., Fernandez, M., Eds.; Cenozoic Fore Land-Basins of Western Europe. Geol. Soc. Spec. Pub., 134: 403–422.
41. Schreiner, A. **1992**. Geol. Karte 1:50.000 Baden-Württ. Erl. Bl. Hegau und westl. Bodensee. Geologisches Landesamt Baden-Württemberg.
42. Schwarz, H.U. **2012**. Das Schwäbisch-Fränkische Bruchmuster. Z. dt. Ges. Geowiss.163/4, 411–446. doi:10.1127/1860-1804/2012/0163-0411.
43. Véron, J. **2005**. The Alpine Molasse Basin-review of petroleum geology and remaining potential. Bull. Angew. Geol. 10: 75–86.
44. Ernst, W. **1969**. Störungsabgrenzungen im Umkreis des Überlinger Sees mit Bodengasen. Bull. Ver. Schweiz. Petrol. -Geol. u. -Ing. 35: 1–11. doi:10.5169/seals-195944.

45. Ernst, W. **1971**. Tektonische Untersuchungen mit der Gasmethode im westlichen Bodenseegebiet und im Tessin bei Lugano (Schweiz). Bull. Ver. Schweiz. Petrol. -Geol. u. -Ing. 37: 37–50.
46. Schreiner, A. **1979**. Zur Entstehung des Bodenseebeckens. Eiszeitalter u. Gegenwart. 29: 71–76.
47. Müller, H.W.; Naef, H.; Graf, H.R. **2002**. Geologische Entwicklung der Nordschweiz, Neotektonik und Langzeitszenarien Zürcher Weinland, Nagra Techn. Ber. ntb 99-08.
48. Pavoni, N., **1984**. Seismotektonik Nordschweiz, Nagra Techn. Ber. ntb 84-45.
49. Deichmann, N.; Ballarin Dolfin, D.; Kastrup, U. **2000**. Seismizität der Nord- und Zentralschweiz, Nagra Techn. Ber. ntb 00-05
50. Mälzer, A.; Rösch, H.; Misselwitz, I.; Ebert, M.; Moosmann, D. **1988**. Höhenänderungen in der Nordschweiz und im Südschwarzwald bis zum Bodensee, NagraTechn. Ber. ntb 88-95.
51. Pfiffner, O.A.; Deichmann, N. **2014**. Seismotektonik in der Nordschweiz. Nagra Arbeitsbericht NAB, 14–26.
52. Vanneste, K.; Verbeeck, K.; Camelbeeck, T. **2012**. A model of composite seismic sources for the Lower Rhine Graben. Poster T33A-2636. AGU Fall Meeting, San Francisco, 3-7 December, 2012.
53. BNS, **2022.** Erdbebenstation Bensberg: Erdbebenkatalog. BNS - Erdbebenstation Bensberg (uni-koeln.de); accessed on 01. August 2022.
54. LGRB, **2022**. Erdbebendienst Südwest - Landeserdbebendienst Baden-Württemberg. LGRB | Erdbeben | Jahresbulletins (lgrb-bw.de); accessed on 01. August 2022.
55. SED, **2022**. Schweizerischer Erdbebendienst (SED). Alle Erdbeben. SED | Alle Erdbeben (ethz.ch); accessed on 01. August 2022.
56. Hinkle, M. **1995**. Concentrations of N_2, O_2, CO_2 and He in Soil Gases Collected over and near the Dixie Valley Known Geothermal Resource Area Northern Dixie Valley, Nevada; Open-File Report 95-0080; U.S. Geological Survey: Reno, NV, USA, 26 p.
57. Baddeley, A.; Rubak, E.; Turner, R. **2015**. Spatial Point Patterns: Methodology and Applications with R. Chapman and Hall/CRC Press.
58. Wickham, H. **2009**. ggplot2: Elegant Graphics for Data Analysis. Springer-Verlag New York.
59. R Core Team. 2015. R version 3.2.2. Available online: https://www.r-project.org/.
60. D'Errico, J. **2010**. Surface Fitting using gridfit. Release 11 Nov 2005 (Updated 29 Jul 2010).
61. Reimann, C.; Filzmoser, P.; Garrett, R.G. **2005**. Background and threshold: critical comparison of methods of determination. Sci. Total Environ. 346: 1– 16. doi:10.1016/J.SCITOTENV.2004.11.023.
62. Tukey, J.W. **1977**. Exploratory data analysis. Reading. Addison-Wesley.
63. Shapiro, S.S.; Wilk, M.B. **1965**. An analysis of variance test for normality (complete samples). Biometrika. 52: 591−611. doi:10.1093/biomet/52.3-4.591. doi: 10.1093/biomet/52.3-4.591.
64. Sinclair, A.J. **1974**. Selection of threshold values in geochemical data using probability graphs. J. Geochem. Expl. 3: 129-149. doi:10.1016/0375-6742(74)90030-2.
65. Sinclair, A.J. **1991**. A fundamental approach to threshold estimation in exploration geochemistry: probability plots revisited. J. Geochem. Expl. 41: 1-22. doi:10.1016/0375-6742(91)90071-2.
66. Risdianto, D.; Kusnadi, D. **2010**. The Application of a Probability Graph in Geothermal Exploration. Proc. World Geothermal Congress 2010. Bali, Indonesia, 25-29 April 2010, 1-6.
67. Edwards, A. L. **1976**. The Correlation Coefficient. Ch. 4. In: An Introduction to Linear Regression and Correlation. San Francisco, CA: W. H. Freeman, 33-46.
68. Ripley, B.D. **1991**. Statistical inference for spatial processes. Cambridge University Press. 154 p.
69. Davidson, T.A.; Emerson, D.E. **1990**. Direct determination of the helium 3 content of atmospheric air by mass spectrometry. J. Geophys Res.: Atmospheres, 95: doi:10.1029/JD095iD04p03565.
70. BfS IMIS. **2022**. www.imis.bfs.de/geoportal, accessed on 23 August 2022
71. Viveiros, F.; Ferreira, T.; Silva, C.; Gaspar, J.L. **2009**. Meteorological factors controlling soil gases and indoor CO_2 concentration: A permanent risk in degassing areas. doi:10.1016/j.scitotenv.2008.10.009
72. LfU-BW. **2003**. Radioaktivität in Baden-Württemberg. Jahresbericht 1998 – 2001. Radioaktivität und Strahlenschutz. Band 7. Landesanstalt für Umweltschutz Baden-Württemberg. 1. Auflage 2003.
73. Hinkle, D.E.; Wiersma,W.; Jurs, S.G. **2009**. Applied Statistics for the Behavioral Sciences, 5th ed.: Wadsworth Publishing: Belmont, CA, USA.
74. Dubois, G. **2005**: An overview of radon surveys in Europe. Luxembourg: Office for Official Publications of the European Communities, EUR 21892 EN -Scientific and Technical Research Series, ISBN 92-79-01066-2. 168 pp.
75. Podugu, N.; Mishra, S.; Wiersberg, T.; Roy, S. **2019**. Chemical and Noble Gas Isotope Compositions of Formation Gases from a 3km Deep Scientific Borehole in the Koyna Seismogenic Zone, Western India. Geofluids. ID 1078942. Doi:10.1155/2019/1078942.
76. Baubron, J.C.; Rigo, A.; Toutain, J.P. **2002**: Soil gas profiles as a tool to characterize active tectonic areas: the Jaut Pass example (Pyrenees, France). Earth and Planetary Sci. Let. 196: 69-81. doi: 10.1016/S0012-821X(01)00596-9.
77. Butt, C.R.M.; Gole, M.J.; Dyck, W. **2000**. Helium. Handb. Explor. Geochem. 7: 303–352.
78. Ammann, M.; Schenker, F. **1989**. Nachweis von tektonischen Störungen in 2 Bodengasprofilen in der Nordschweiz. Nagra Techn. Ber. ntb 89-25.

79. Chiodini, G.; Frondini, F.; Ponziani, F. **1995**. Deep structures and carbon dioxide degassing in Central Italy. Geothermics 24: 81-94. doi:10.1016/0375-6505(94)00023-6.
80. Etiope G.; Lombardi, S. **1995**. Evidence for radon transport by carrier gas through faulted clays in Italy. J. Radioanaly. Nuc. Chem. 193: 291-300. doi: 10.1007/BF02039886.
81. Voltattorni, N.; Cinti, D.; Pizzino, L.; Sciarra, A. **2014**. Statistical approach for the geochemical signature of two active normal faults in the western Corinth Gulf Rift (Greece). Appl. Geochem. 51: 86–100. doi:10.1016/J.APGEOCHEM.2014.09.011.
82. Voltattorni, N.; Lombardi, S.; Beaubien, S.E. **2015**. Gas migration from two mine districts: The Tolfa (Lazio, Central Italy) and the Neves-Corvo (Baixo Alentejo, Portugal) case studies. J. Geochem. Expl. 152: 37-53. doi:10.1016/J.GEXPLO.2015.01.011.
83. Viveiros, F.; Gaspar, J.L.; Ferreira, T.; Silva, C.; Marcos, M.; Hipólito, A. **2015**. Mapping of Soil CO_2 diffuse degassing at São Miguel Island and its public health implications., Azores archipelago: Volcano monitoring perspectives. Chapter 14. In: J.L. Gaspar, J.E. Guest, A.M. Duncan, F.J.A.S. Barriga, D.K. Chester (eds). Volcanic Geology of São Miguel Island (Azores Archipelago).
84. Amundson, R.G.; Davidson, E.A. **1990**. Carbon dioxide and nitrogenous gases in the soil atmosphere. J. Geochem. Explor. 38: 13–41. doi: 10.1016/0375-6742(90)90091-N.
85. Büchi, U.P.; Schlanke, S.; Müller, E. **1976**. Zur Geologie der Thermalwasserbohrung Konstanz und ihre sedimentpetrographische Korrelation mit der Erdölbohrung Kreuzlingen. Bull. Ver. Schweiz. Petroleum-Geol. u. -Ing., 42: 25-33.
86. Ciotoli, G.; Bigi, S.; Tartarello, C.; Sacco, P.; Lombardi, S.; Ascione, A.; Mazzoli, S. **2014**. Soil gas distribution in the main coseismic surface rupture zone of the 1980, Ms = 6.9, Irpinia earthquake (southern Italy), J. Geophys. Res. Solid Earth, 119: 2440–2461, doi:10.1002/ 2013JB010508.
87. Baubron, J.C.; Allard, P.; Toutain, J.P. **1990**. Diffuse volcanic emissions of carbon dioxide from Vulcano Island, Italy. Nature. 344: 51-53. doi: 10.1038/344051a0.
88. Pfanz. H.; Saßmannshausen. F. **2008**. Geogenic CO_2-Exhalations and Vegetation: Its possible use to predict volcanic eruptions. Geophysical Research Abstracts 10: EGU2008-A-12108.
89. Burkhard, M.; Grünthal, G. **2009**. Seismic source zone characterization for the seis-mic hazard assessment project PEGASOS by the Expert Group 2 (EG1b). Swiss J. Geosci. 102: 149–189. doi: 10.1007/s00015-009-1307-3.
90. Das, N.; Chandran, P. **2011**. Microbial Degradation of Petroleum Hydrocarbon Contaminants: An Overview. Biotechnol. Res. Internat. ID 941810, doi:10.4061/2011/941810
91. Fleet, A. J.; Wycherley, H.; Shaw, H. **1998**. Large volumes of carbon dioxide in sedimentary basins. Mineralogical Magazine. 62A: 460-461. doi: 10.1180/MINMAG.1998.62A.1.244.

Compilation of tectonic structures

10, 36, 52

Earthquake catalogues on the Internet

53-55